2022

Cloud Radiative Effects on MJO Development in DYNAMO

Qi Hu

Zihang Han

Shuguang Wang

Published (2022) Journal of Climate, 35 (21), pp. 3369-3384.

Cloud Radiative Effects on MJO Development in DYNAMO

QI HU,[a] ZIHANG HAN,[b] AND SHUGUANG WANG[c]

[a] *School of Natural Resources, and Department of Earth and Atmospheric Sciences, University of Nebraska–Lincoln, Lincoln, Nebraska*
[b] *College of Atmospheric Sciences, Lanzhou University, Lanzhou, China*
[c] *School of Atmospheric Sciences, Nanjing University, Nanjing, China*

(Manuscript received 17 November 2021, in final form 18 June 2022)

ABSTRACT: Observed Madden–Julian oscillation (MJO) events are examined with the aid of regional model simulations to understand the role of cloud radiative effects in the MJO development. The importance of this role is demonstrated by the absence of the MJO in the model simulations that contain no cloud radiative effects. Comparisons of model simulations with and without the cloud radiative effects and observation help identify the major processes arising from those effects. Those processes develop essentially from heating in the upper troposphere due to shortwave absorption within anvil clouds in the upper troposphere and the convergence of longwave radiation in the middle to upper troposphere, with a peak at 300 hPa, during deep convection. First, that heating adds extra buoyancy and accelerates the rising motion in the upper troposphere in deep convection. The vertical acceleration in the upper troposphere creates a vacuum effect and demands for more deep convection to develop. Second, in response to that demand and required by mass balance arises the large-scale horizontal and vertical mass, moisture, and energy convergence. It strengthens deep convection and, with the feedback from continuing cloud radiative effect, creates conditions that can perpetuate deep convection and MJO development. That perpetuation does not occur however because those processes arising from the cloud radiative heating in the upper troposphere stabilize the troposphere until it supports no further deep convection. Weakening deep convection reduces cloud radiative effects. The subsequent reduction of the vacuum effect in the upper troposphere diminishes deep convection completing an MJO cycle. These results advance our understanding of the development of the MJO in the radiative–convective system over warm waters in the tropics. They show that while the embryo of intraseasonal oscillation may exist in the system its growth/development is largely dependent on cloud radiative effects and feedbacks.

KEYWORDS: Madden-Julian oscillation; Cloud radiative effects; Tropical variability

1. Introduction

The Madden–Julian oscillation (MJO; Madden and Julian 1971) is a quasi-periodic variation in deep convection, precipitation, and associated atmospheric circulation over the warm pool areas of the tropical Indian Ocean and the western Pacific Ocean. While deep convection in the MJO is mostly confined to the warm pool areas, waves related to the MJO propagate in the tropical atmosphere and even extend to the midlatitudes. The MJO has a frequency range of 20–90 days with a peak in power at 30–50 days per cycle. Because the MJO has reported effects on significant weather and climate events of regional to global scales, including tropical cyclones (e.g., Maloney and Hartmann 2000), monsoons (e.g., Wheeler and McBride 2005; Duan et al. 2019), and El Niño (e.g., Takayabu et al. 1999), and because its intraseasonal time scale has a potential for improving extended predictions on global weather and climate (e.g., Waliser et al. 2003), its initiation and development have been intensely studied in the past five decades. In the course of these studies, many processes have been identified and shown to influence MJO development, as summarized in Wang (2005) and Zhang et al. (2020). Among them are interactions of evaporation in the warm pool region with large-scale atmospheric dynamics through the planetary boundary layer (Emanuel 1987; Neelin et al. 1987; Wang and Li 1994; Sobel et al. 2010), the influence of extratropical processes such as westerly wind bursts (e.g., Webster 1983; Ray and Zhang 2010), amplifying tropical atmospheric waves modified by deep convection-induced heating (e.g., Lau and Peng 1987; Wang 1988), interactions of radiation and convection (clouds) over tropical warm waters (Hu and Randall 1994, 1995; Raymond 2001; Bony and Emanuel 2005; Khairoutdinov and Emanuel 2018; Benedict et al. 2020), and others focusing on specific aspects of these processes from water and energy balance perspectives (e.g., Bladé and Hartmann 1993; Sobel and Maloney 2012).

While all these mechanisms play certain roles in MJO development (Zhang et al. 2020), some of them play a more dominant role in some events and different interplays among those processes lead to the development of some other events. This subtle yet critical shift of the major processes in individual MJO development, dependent on large-scale circulation conditions at the time, could explain the wide spectrum of the MJO (20–90 days per cycle) and its elusive nature, as also implicated by the significant difficulties in simulating the MJO in numerical models (e.g., Miura et al. 2007; Kim et al. 2014).

Denotes content that is immediately available upon publication as open access.

Supplemental information related to this paper is available at the Journals Online website: https://doi.org/10.1175/JCLI-D-21-0882.s1.

Corresponding author: Dr. Qi Hu, qihu@unl.edu

DOI: 10.1175/JCLI-D-21-0882.1

In this study, we further investigate the roles of interactions of radiation and convection (clouds) in the development of the MJO, using observed cases. Radiation and convection (clouds) play an important role in the variation of the column-integrated moisture static energy (MSE) in the tropical atmosphere, and such variation can lead to instability in the development of intraseasonal oscillations (e.g., Hu and Randall 1994, 1995; Kim et al. 2009; Maloney et al. 2010; Andersen and Kuang 2012; Sobel et al. 2014; Kim et al. 2014). Although this instability mechanism has been integrated in our growing understanding of MJO initiation and development in the context of moisture dynamics in the tropical warm water regions (e.g., Ma and Kuang 2016; Zhang et al. 2020), key questions remain on how the interactions of radiation and convection regulate temperature and moisture in the tropical warm water regions to result in their cohesive variations of intraseasonal time scale. Many studies have been intended to understand such roles. For example, Hu and Randall (1994, 1995) showed that intraseasonal oscillations can emerge as a result of the destabilization of atmospheric temperature profile by radiation competing with stabilization of the profile by convection. The time scale of the oscillation is dependent on the atmospheric radiative cooling rate. It remains unexplained how the cooling rate is determined by the interaction of radiation and convection/cloud. More recent studies have used mechanism-denial experiments in global models to isolate the effect of radiation–convection interaction on MJO development (e.g., Kim et al. 2011; Wang et al. 2013, 2016; Ma and Kuang 2016). Ma and Kuang (2016), for example, used the Superparameterized Community Atmosphere Model and compared its control run result with results of several mechanism-denial experiments while preserving the same mean state among the runs. In their experiments, only the one with denied radiation–convection interaction had no MJO signals. While their results show a critical role of the radiation–convection interaction in the MJO development in their global model, they fall short as to how this effect is achieved and if the same role is present in observed cases. Thus, the processes and feedbacks arising from the convection–radiation interaction and MJO development remain unexplained.

In this study, we will examine and identify the processes and feedbacks arising from the cloud radiative effects and contributing to the development of MJO (leaving the propagation of MJO signal in a separate study). We show these processes and feedbacks using the observed MJO events that were recorded during the field campaign of DYNAMO/CINDY2011 (Yoneyama et al. 2013). To identify these processes and feedbacks, we use a recently modified version of the Weather Research and Forecasting (WRF) Model capable of simulating those observed MJO events (Wang et al. 2015). The model and the data that are used to drive and validate against the model control simulation are described in section 2. In section 3, after demonstrating the consistency of the model in describing the observed MJO events we describe model experiments with changes to the model's cloud radiative effects. Results of the model experiments are compared to the control and observation in section 4 to show the roles of the cloud radiative effects and feedbacks in amplifying and sustaining deep convection in the development of the MJO. A summary of this work along with an implication in MJO propagation is presented in section 5.

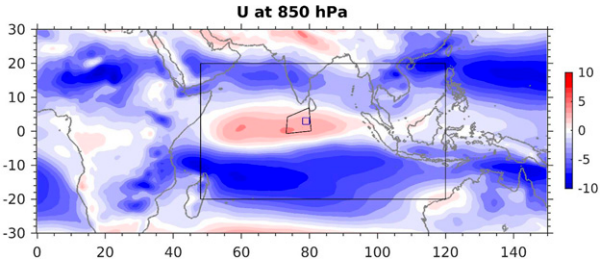

FIG. 1. The model domain is shown by the black rectangular box. The DYNAMO IOP NSA is shown by the black polygon. The blue square box inside the polygon is the area where detailed analyses are conducted in this study. The background field in color is the 850-hPa zonal wind averaged from October to December 2011 (units: m s^{-1}).

2. Data and methods

a. Data

We use two sources of data. Group 1 has datasets that are used to derive the initial and boundary conditions of the regional model in its simulations and experiments. Datasets in group 1 are ERA5 data (Hersbach et al. 2020) and ERA5 sea surface temperature (SST) data. Group 2 has datasets derived from field observations, including precipitation, surface evaporation, and radiation. These data are developed from the field campaign of the DYNAMO/CINDY2011 and the Atmospheric Radiation Measurement (ARM) MJO Investigation Experiment (AMIE). The observations in the DYNAMO campaign were taken over the tropical Indian Ocean from 1 October 2011 to 31 March 2012, with an intensive observing period (IOP) from 1 October 2011 to 15 January 2012. Data from the IOP in the Northern Sounding Array area (NSA; shown by the black polygon in Fig. 1) are used, where two well-organized MJO events were observed and documented. These observations along with the AMIE data will be collectively referred to as DYNAMO data in this study.

As described in detail in Ciesielski et al. (2014), these data in group 2 have large-scale winds, geopotential height, and air temperature that were extracted from the gridded (resolution of 1° × 1°) sounding-based DYNAMO IOP products with 3-h and 25-hPa resolution. Atmospheric relative humidity is derived from the NSA dataset (Johnson and Ciesielski 2013). Surface evaporation data are from those collected by the R/V *Roger Revelle* during the DYNAMO IOP. The atmospheric downwelling longwave radiation flux at the surface was measured on board on DYNAMO cruise legs 2 and 3. The SST measured at 1-m depth at the D1 mooring (0°N, 78.9°E) is used to represent the SST in our focused area of analysis at 2°–4°N, 78°–80°E, the blue square box in Fig. 1. Precipitation data are from the 3-hourly 0.25°-resolution TRMM-3B42-7A

dataset (Huffman et al. 2007). These data are used in model validation.

b. Model

The numerical model used in this study is the modified version of the WRF v3.8.1 by Wang et al. (2015) capable of simulating the MJO events in DYNAMO. Applying this regional model to simulate the MJO allows us to focus on regional processes important to the MJO while sustaining a consistent atmospheric circulation in the model domain with the observed global circulation through lateral and lower boundary conditions (Wang et al. 2015). Although there is no feedback from processes in the regional model to outside circulations, its potential impacts on the MJO development are expected to be small because the cloud–radiation interaction examined in this study is a local/regional process and occurs only when there is deep convection.

Our regional model domain is from 20°S to 20°N and from 48° to 120°E (black rectangle domain in Fig. 1). The horizontal grid spacing is 9 km. There are 45 vertical levels in the model, with 9 levels in its lowest 1 km and a nominal top at 20 hPa. Near the center of the domain is the NSA of DYNAMO (black polygon in Fig. 1).

Model physical processes include surface water and energy budgets, atmospheric boundary layer turbulent mixing, cloud microphysics, and solar and longwave radiation transfer in the atmosphere. They are described in detail in Wang et al. (2015), so are not repeated here. It is important to note that this model uses no convection parameterization and describes convection explicitly. Although at the 9-km grid spacing the model cannot simulate individual cumuli it can appropriately describe convective systems on scales of 16 km and larger. By not using parameterization for convection in the model, we avoid the sensitivity of model simulated MJO to convective parameterization methods. Such sensitivity has been the focus of many studies and is, in nature, describing the sensitivity of model MJO to convection and cloud–radiation interaction because different convective parameterizations place clouds generated in convection along their specified vertical profiles that would interact with both solar and longwave radiation differently and likely result in different outcomes of their simulated MJO. By not using convective parameterization, we allow convection/cloud to interact with radiation freely so to remove one constraint on model processes affecting MJO initiation and development.

Lateral boundary conditions of the model are derived using the ERA5 data and updated every 6 h in model runs. Next to the lateral boundary of the model is a narrow transition zone of five model grid points into the interior (Skamarock et al. 2008). Over those five rows/columns of grids the tendencies of boundary values are transitioned to affect the tendencies in the model. This device, equivalent to a nudging along the boundaries using the reanalysis data, is used to ensure the transition of the large-scale forcing from the hydrostatic dynamics of the ERA5 model to the nonhydrostatic solution of the WRF Model. Lower boundary conditions over land areas in the model domain are specified by the ERA5 data only at the initial time. Over oceanic areas, the SST at model grids is assigned initially and updated every 6 h using ERA5 SST data.

The same lateral and lower boundary conditions are used in the model simulation of the MJO events during the DYNAMO IOP and in model experiments. Thus, the large-scale circulation condition imposed on the model domain is the same in model experiments as in model control simulation. The difference between their results will therefore show the roles of processes inside the regional model in the development of the MJO events.

3. Model validation and experiments

a. Validation

Because this model has successfully simulated the two MJO events in the DYNAMO IOP (Wang et al. 2015, hereafter WSZSYZ), our validation of the model is to repeat the simulation of those events. This validation is necessary to assure that the model simulations are not affected because of our use of the recently upgraded ERA5 data (ERA-Interim data were used in WSZSYZ). As in WSZSYZ, a spectral nudging is applied to horizontal winds on the first three days of model simulation. The effect of this nudging is to relax the large-scale horizontal winds, wavenumbers 0–4 in zonal and wavenumbers 0–2 in meridional winds, in the model domain to the ERA5 winds. It aims to reinforce the large-scale dynamics contained in the initial condition so that the model simulation can continue with the correct and relevant major global-scale dynamic elements.

Figures 2a and 2c show the model simulated 3-hourly and daily surface precipitation, respectively, from 1 October to 15 December 2011 in the region 0°–5°N, 50°–120°E. The variation of simulated precipitation is consistent with the observation derived from the TRMM data, shown in Figs. 2b and 2d, although the intensity is slightly weaker. Two distinctive MJO events are described in the model simulation. The intensity and variation of the simulated precipitation are identical to that in WSZSYZ. Additional analyses of our simulated dynamic and moisture processes during the simulated MJO are compared to those detailed in WSZSYZ. They are nearly identical. This consistency between these simulated and observed MJO events during the DYNAMO and between our results and those of WSZSYZ justify our use of this modeling system to further investigate the roles of cloud radiative effect on the MJO development. In the following discussions, we will refer these simulated MJO events as the control results of the model (CTRL). The CTRL will be compared and contrasted against the results of the model experiments with changes in cloud radiative effect. These experiments are described next.

b. Experiment design and rationale

To examine the roles of cloud radiative effect in the development of the two observed MJO events we conduct two experiments, EXP1 and EXP2. In EXP1, clouds at and above 600 hPa in the model are rendered transparent to the solar

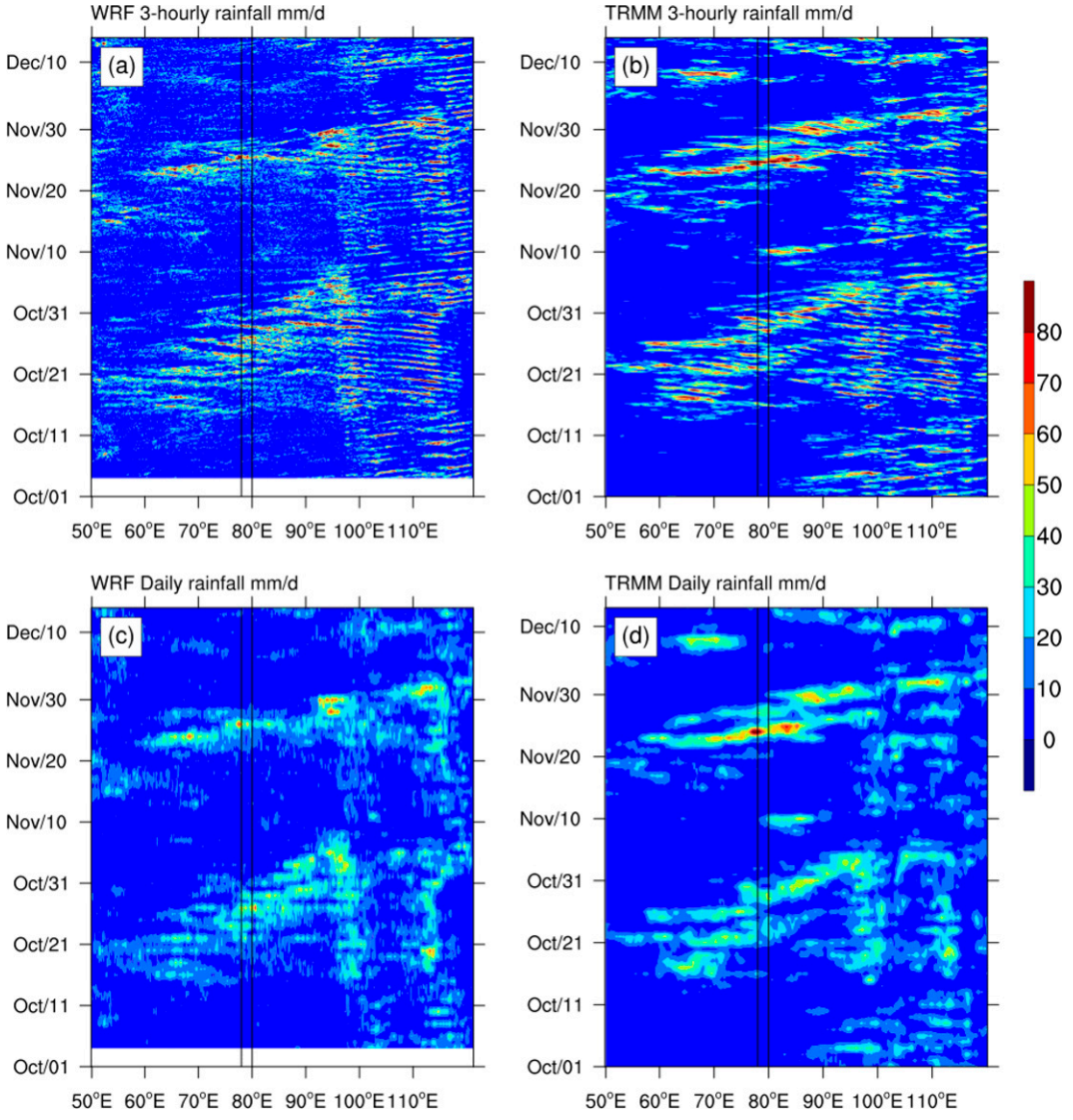

FIG. 2. Time–longitude diagram of control results of (a) 3-hourly and (c) daily rainfall rate and observed (b) 3-hourly and (d) daily rainfall rate (units: mm day^{-1}) from October to December 2011. The two vertical black lines encompass the longitude band of the area of our detailed analysis.

and longwave radiation. EXP2 is similar to EXP1 except that all clouds in the model atmospheric column are rendered transparent to the radiation. The lateral and lower boundary conditions in EXP1 and EXP2 are the same as in the CTRL. In these experiments, convection still develops and deep clouds form. They just do not interact with the solar and longwave radiation. To reduce the sensitivity of model internal processes and model solution to the initial condition, we use the ensemble solution of each experiment. Each ensemble solution is derived from six members. They are from simulations using initial condition and corresponding boundary conditions taken from the observation 3 h after the previous one, with the first one starting at 0000 UTC 1 October 2011. Ensemble means of the six members are calculated and used in our analyses and comparisons to the CTRL.

The rationale for EXP1 and EXP2 is the following. Clouds redistribute the solar and longwave radiation (LWR) in the atmosphere. Clouds in the upper troposphere, such as anvil clouds from detrainment of deep convection, have very cold cloud-top temperatures. They effectively reduce upward LWR at the altitude of the cloud top and, hence, shield the LWR loss from cloud layers underneath. The net effect of these processes is a convergence of LWR that increases the temperature in the middle to upper troposphere. This cloud LWR effect is most efficient over warm water regions in the tropical Indian Ocean and the western Pacific Ocean region for two reasons (Sherwood et al. 1994). One is the high SST that emits large LWR, which will be absorbed at the base and the lower portion of anvil clouds. The other is that the deep convection in the region creates very high cloud tops with

very cold cloud-top temperatures. The resulting strong LWR convergence and heating in the middle- to upper-troposphere clouds is further enhanced by the net absorption of solar radiation by cloud ice particles. These radiation effects of clouds in the middle to upper troposphere can reach up to 100 W m^{-2}, essential to balance the atmospheric energy in the tropical warm pool region (e.g., Stephens and Webster 1979).

Meanwhile, reflection and scattering of solar radiation by clouds reduces the amount of solar radiation reaching the surface. This reduction of solar radiation at the surface can be as large as -100 W m^{-2} (e.g., Sherwood et al. 1994). Although the effects of clouds on solar radiation and LWR nearly balance when they are integrated in the Earth–atmosphere column in the tropical warm pool region, they affect the vertical profile of the atmospheric temperature and static stability very differently. A large portion of the solar radiation deposited at the surface in cloud-free condition over time is transformed to LWR and converged to the upper troposphere during deep convection. Although this process leaves a near balance of the column-integrated net radiation at seasonal and longer time scales (Stephens and Webster 1979), it involves rather dynamic components of energy conversion and redistribution in the atmosphere in subseasonal scales. The energy redistribution in this process has been suggested to play an important role in intraseasonal variations and the MJO in the tropical warm water regions (Hu and Randall 1994, 1995) and supported by observed consistent phase relationship between MJO precipitation and variation of column-integrated MSE (e.g., Lin and Mapes 2004; Ma and Kuang 2011).

When these cloud radiation effects are removed in EXP1/EXP2 a large part of vertical redistribution of energy in the surface–atmosphere column is interrupted and the associated dynamic processes, such as vertical motion, weaken or are replaced by different forces (e.g., subsidence). If these processes and the energy redistribution driven by the cloud radiative effects are responsible for (or described/manifested by) MJO development in the equatorial Indian and western Pacific Ocean region, their absence will result in the absence of the MJO.

We acknowledge that there have been concerns of influences on the model results including the MJO from possible model mean state shift in mechanism-denial experiments using global models [e.g., Ma and Kuang (2016) and references therein]. Possible influences on the mean state of our regional (finite area) model from removing the cloud radiative effects are small because 1) the eigenvalues/modes (basic state) of finite-area models (a boundary-value problem) are primarily determined by their boundary conditions (e.g., Cahill 2013). These boundary conditions in our regional model simulations are updated every 6 h using the ERA5 data, forcing the large-scale circulation or basic state of the model to be consistent with observed global circulation. To a certain extent, this is similar to using the nudging method in Ma and Kuang (2016) to keep a similar basic state in their simulations using a global model. 2) The removal of the cloud radiative effects in our experiments can be considered as a pulse of force in the governing equations of the model that counters the cloud radiative effect only when deep convection occurs in the model; the force is absent in clear sky and shallow convection conditions in the experiments. Thus, the model results show primarily the responses of the same basic state to that pulse of force when convection occurs.

4. Results and discussion

In this section, we examine the observation and the CTRL results and describe the major processes arising from the cloud radiative effects of both solar and longwave radiation and influencing the development of the two MJO events observed during the DYNAMO. These processes are identified by the differences of the results between the CTRL and the ensemble results of EXP1 and EXP2. In describing these processes and their rise from the cloud radiative effects we use this following set of variables: atmospheric temperature (T), precipitation at the surface (Pr), downward LWR (LWR) at the surface, the average of relative humidity (RH) in the lower troposphere from the surface to 850 hPa, and a normalized atmospheric lapse rate defined as $\Gamma_N = (\Gamma - \Gamma_m)/(\Gamma_d - \Gamma_m)$ (Arakawa and Chen 1987), where Γ_m and Γ_d are the moist and dry adiabatic lapse rate, respectively, and the actual lapse rate Γ is calculated from the temperatures at 1000 and 300 hPa and the physical distance between the two pressure levels. The value of Γ_N varies between 0 and 1; it is close to 1 when the lapse rate is steep and near Γ_d, and close to 0 when the lapse rate is less steep and near Γ_m. As shown in the observational work of Arakawa and Chen (1987), Γ_N and RH have a negative relationship in the tropical atmosphere, which describes the role of deep convection/cloud in sustaining the temperature and moisture profiles of the tropical atmosphere.

a. CTRL results

Figures 3a and 3b show the temporal variations of Pr, RH, LWR, and Γ_N from the CTRL. Their values are averaged over the blue square box in Fig. 1. The phases of the variations of these variables and their averaged values over the two simulated MJO events (given in the figure legend) are very close to the observed, shown in Figs. 3c and 3d. The phase variations show that in the MJO events during DYNAMO the moisture/RH increases in the lower troposphere before the start of intense convection (Pr). Meanwhile, the atmospheric lapse rate Γ_N decreases, a reflection of the moist convective adjustment by shallow convection (Figs. 3a,c). The lapse rate decreases sharply following the start of intense convection/Pr and eventually arrives at its minimum value in each of those events. The decreasing/small lapse rate during the period of deep convection occurs in conjunction with increasing/high RH. After the period of intense convection/Pr, the RH decreases while the lapse rate increases.

Some important physical processes driving these alternations between steep lapse rate/low RH with little convection and less steep lapse rate/high RH during intense/deep convection in the life cycle of the MJO events are suggested by the results in the Γ_N–RH diagram of Fig. 4. The utility of this diagram in helping our comprehension of the MJO development is that it focuses on the interaction of radiation and

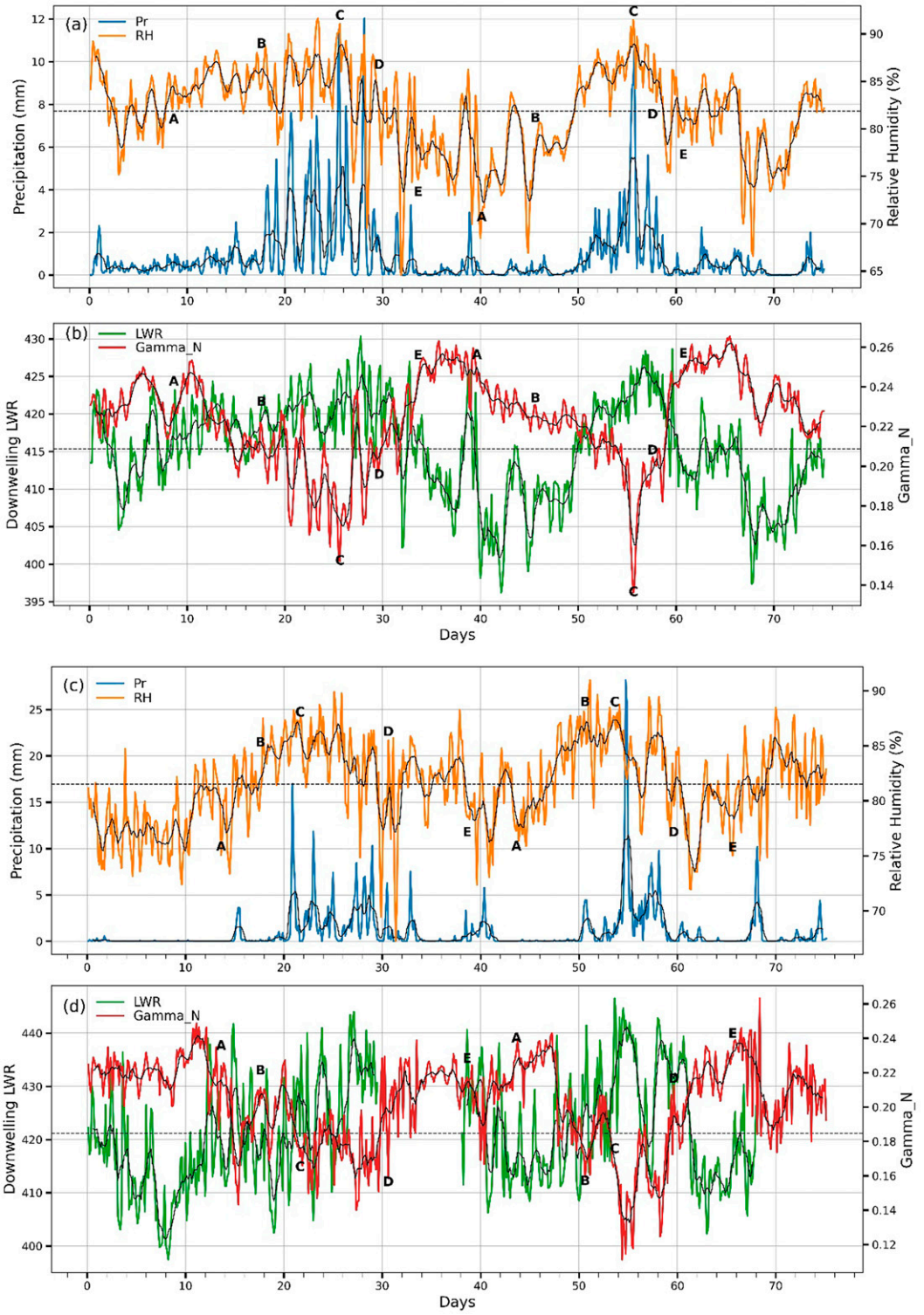

FIG. 3. (a),(b) CTRL and (c),(d) observed 3-hourly time series of model physical variables from 1 Oct (day 0) to 15 Dec (day 75) 2011. All results are averaged over the blue square box in Fig. 1. The thin black solid line in the time series of each variable is its eight-value running mean. The dashed line in (a) and (c) shows the time average of RH (81.84% in CTRL and 81.50% in the observation). The dashed line in (b) and (d) shows the average downwelling LWR, which is used in calculations of LWR anomaly in peak convection (415.3 W m^{-2} in CTRL and 421.1 W m^{-2} in the observation). The average precipitation is 7.1 and 7.9 mm day^{-1} in CTRL and the observation, respectively. The average Γ_N is 0.22 and 0.20 in CTRL and the observation, respectively. The uppercase letters A to E in the set of CTRL and the observed panels mark the time when the atmospheric conditions during the two MJO events are examined in the Γ_N–RH diagram in Fig. 4.

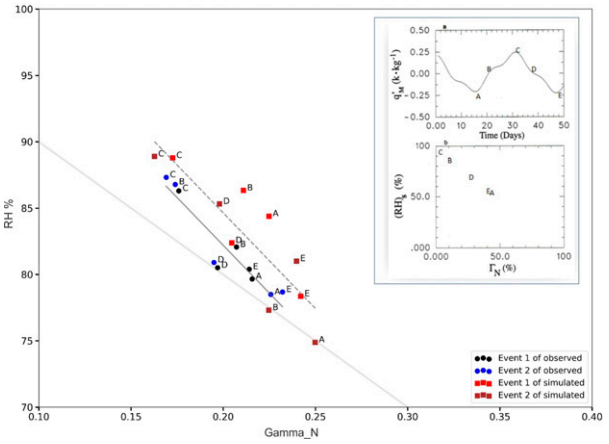

FIG. 4. Observed and CTRL results of variations of thermodynamic conditions of the atmosphere in the Γ_N–RH diagram during the two MJO events. Each event is sequenced from A to E by the same-colored symbols. The sequence of A to E in each observed or simulated MJO event is shown in Fig. 3. The light gray line shows the -1 diagonal ($y = 1 - x$) of the Γ_N–RH diagram. The solid and dashed black lines show the regression relationship of RH and Γ_N for the observed and CTRL, respectively, in the data series presented in Fig. 3. The inset shows the low-frequency variation of mixed layer mixing ratio in (a) (similar to RH in Fig. 3), and the variation depicted in the Γ_N–RH diagram in (b) from the theoretical radiative–convective model of Hu and Randall (1995, see their Fig. 10).

convection in the development of the MJO. In the Γ_N–RH diagram, the change of tropical atmospheric condition along the horizontal Γ_N axis is caused primarily by radiation and convection. For instance, in clear-sky conditions, strong solar heating at the surface and LWR cooling in the upper troposphere steepen the lapse rate, moving the condition of the atmosphere to the right with large Γ_N. Convection reduces the lapse rate to meet the static stability constraint under a given moisture content (Manabe and Strickler 1964) by releasing a certain amount of latent heat and associated large-scale compensating subsidence that warms the middle and upper troposphere. Meanwhile, the radiative effect of clouds (anvils) from deep convection warms the upper troposphere (section 3b) and reduces the lapse rate, thus moving the condition to the left with smaller Γ_N.

Along the vertical RH axis in the Γ_N–RH diagram, convection can increase atmospheric moisture by enhancing horizontal moisture convergence (e.g., Fig. 13 in WSZSYZ), moving the atmospheric condition up in the diagram. After the peak phase of convection when the atmosphere convective stability increases, the net effect of weakening convection is to further reduce atmospheric moisture by condensation and precipitation, moving the condition down to lower RH in the diagram. Meanwhile, weak subsidence continues and dries the atmosphere.

The presence of these processes of radiation and convection and their interaction and feedback (collectively cloud radiative effects) in the development of the MJO are indicated by letters A to E in Fig. 4. They show the sequence/variation of the atmospheric state in the Γ_N–RH diagram in the life cycle of each of the observed and simulated MJO events (see the same letters marked in the time series in Fig. 3). Although there are differences in the exact timing/dates of the phases A to E between the observed and the CTRL in the diagram, the evolution of the atmospheric condition from A to E described by the CTRL mimics the observed. When all points in the simulated (observed) time series shown in Figs. 3a and 3b (Figs. 3c,d) were plotted in Fig. 4, the data points were scattered along and in proximity to the dashed (solid) black line in Fig. 4. To focus on the evolution of atmospheric condition during the MJO events we show those selected five states representing the major phases in the MJO events: 1) initiation phase from A to B, 2) stabilization phases from B to C, and to D, and 3) relaxation and a follow-up destabilization phase from D to E. These phases and corresponding states were selected based on the evolution described in Fig. 3 so as to best describe the MJO development in the Γ_N–RH diagram.

In the beginning of the MJO events, the atmosphere is at condition A or E in the diagram with low RH (drier) and high Γ_N (steeper lapse rate). With little cloud, strong solar insolation encourages surface evaporation in the warm pool region (shown in the surface energy budget of the events in Fig. 8a later). Increasing moisture pushes the atmosphere state to higher RH (upward in the diagram). Meanwhile, increasing surface energy intensifies turbulence in the planetary boundary layer and initiates shallow convection (e.g., Khairoutdinov and Randall 2006), pushing the state to the left in the diagram with reduced Γ_N. Their combined effect is to move the atmosphere along the solid or dashed black line in Fig. 4 toward state B. These processes continue until deep convection starts after additional moistening (rising RH) and the rise of instability for deep convection and subsequently cloud radiative effect in the troposphere (demands for smaller Γ_N in higher RH; e.g., Manabe and Strickler 1964). In the developing phase of the MJO, shown by the sharp increase of Pr in Figs. 3a and 3c, there are large changes/jumps of both RH and Γ_N from B to C in Fig. 4 (in the observed event 2, the jumps occurred at an earlier time, but showed the same large changes). The value of Γ_N decreases sharply (stabilization), contemporaneous with the large increase of atmospheric moisture.

After this period of convective stabilization, convection weakens as indicated by the decrease of Pr in Fig. 3. As we will further elaborate later, at the end of this very dynamic period of deep convection the process that converges moisture to the region weakens following the weakening of deep convection as a result of its own feedback to stabilize the atmospheric profile. With a stable lapse rate and weakening convection and moisture convergence, the atmosphere returns to the conditions D and E.

It is intriguing that these variations of the condition of the troposphere described in the Γ_N–RH diagram in Fig. 4 for the two observed and simulated MJO events in DYNAMO share strong similarities with the results shown in the inset of Fig. 4 describing the intraseasonal oscillation obtained from a single-column model that only contains radiation, convection (including cloud radiative effect), and surface evaporation [Hu and Randall 1995; additional and nearly identical variations as the observed/CTRL in Fig. 4 are found in other cases

in Hu (1992)]. Such strong similarities suggest that convection and radiation and their interaction play a critical role in the observed MJO development. Although moisture supply is required in supporting the oscillation it can be from multiple processes (thus not unique), such as surface evaporation, which is the only source in the single column radiative–convective models (Hu and Randall 1994, 1995), or both the surface evaporation and large-scale moisture convergence from dynamic processes associated with deep convection in the observed MJO events (elaborated later).

What are the processes arising from the interactions of convection/cloud and radiation that play such a deterministic role for the MJO development? To identify those processes, we examine the results from the model experiments, focusing on EXP1 in which clouds at and above 600 hPa are rendered transparent to solar and longwave radiation, and compare them to the CTRL and observations.

b. *Cloud radiative effect on enhancing deep convection*

Figures 5a and 5b show the ensemble results of EXP1 for the same variables as the CTRL and observation in Fig. 3. Because the results of EXP2 are nearly identical to EXP1 (as shown in Fig. 6), we will focus our following discussions on the results of EXP1. Our statistical evaluation of the results in Figs. 5a and 5b indicates no identifiable MJO signal in those variables. (Our statistical tests were done using power spectral/Fourier analysis of signals in model outputs followed by a red noise test of the power spectra. The same method is used for similar tests in this study.) This outcome is in clear contrast to the results of the CTRL in Figs. 3a and 3b. Because the cloud radiative effect is the only difference between the CTRL and EXP1 it should be the root cause of the difference between their results. We note that outside the active MJO periods all the variables in EXP1 recover with similar variations as in the CTRL, a result indicating that the cloud radiative effect is limited to the deep convective phase of the MJO.

It is important to note that although there is no detectable MJO signal in the time series shown in Figs. 5a and 5b there are visible shallow cloud bands with resemblance of MJO in the warm pool region as shown in Figs. 5c and 5d from EXP1. These bands of shallow and weak clouds/precipitation likely depict embryos of intraseasonal oscillation similar to that shown in Hu and Randall (1994). In their single-column models intraseasonal oscillations appeared and were shown by variations in precipitation at the surface and clouds in the lower troposphere. Those oscillations were weak yet detectable (statistically significant) largely because of the absence of other signals and variations such as large-scale circulations and interactions, which were not included in their single-column models. Moreover, because those models in Hu and Randall (1994) included no cloud radiative effects their intraseasonal oscillations arose essentially from the radiation destabilization competing with convection stabilization in the atmosphere over warm waters. Those intraseasonal oscillations could be the "embryo" of the MJO but not the MJO itself. The work of Hu and Randall (1994) showed that such an embryo can form in the process of the radiation destabilization and convection stabilization with the presence of a moisture source. We also note that the theoretical model presented in Hu and Randall (1995) did parameterize cloud radiative effects through the use of the observed Γ_N–RH relationship of Arakawa and Chen (1987). The parameterization however limited the possibility to understand cloud radiative effects on the MJO development. The resemblance of the intraseasonal oscillation in Figs. 5c and 5d from EXP1 (and EXP2) suggests that the embryos of such oscillations can form in radiative–convective systems. The difference between the results in Figs. 5c and 5d and the CTRL in Figs. 3a and 3b indicates an important role of cloud radiative effects for the embryos of intraseasonal oscillation to grow into full-scale MJO events.

To understand how the cloud radiative effects may have helped grow the embryo of intraseasonal oscillation and initiated and sustained deep convection development and the MJO, we first examine the cloud radiative effects on the atmospheric temperature profile, alluded to by the results in Fig. 4. Figure 6a shows the domain- and time-averaged difference of the temperature profile between CTRL and EXP1 ($\Delta T = T_{\mathrm{EXP1}} - T_{\mathrm{CTRL}}$). The term ΔT is primarily the difference during the convective phase of the MJO events because the profiles of T_{CTRL} and T_{EXP1} are similar in cloud-free conditions (no cloud effect). The difference in Fig. 6a indicates that the CTRL (with cloud radiative effects) has warmer temperature in the middle to upper troposphere. The temperature is ~1°C warmer around 300 hPa in the CTRL than in EXP1/EXP2. Their difference is minor below 600 hPa, indicating trivial radiative effect of clouds in the lower troposphere. The minor role of clouds below 600 hPa is further shown by the difference of ΔT profiles between EXP1-CTRL and EXP2-CTRL in Fig. 6a. Because EXP1 has no radiative effects for clouds at and above 600 hPa and EXP2 has no radiative effects for all clouds their temperature difference also shows the radiative effects of clouds below 600 hPa. The minor differences between the two profiles in Fig. 6a thus show a trivial radiative effect of those low clouds. This result is consistent with that found in Sherwood et al. (1994) and the more recent work of Zhang et al. (2019).

In Fig. 6a, the much warmer temperature in the middle to upper troposphere in the CTRL than the temperature in EXP1/EXP2 results primarily from net radiation convergence in clouds (cloud radiative effect), shown in Fig. 6b. As in Fig. 6b, there is strong heating in the CTRL simulation, in contrast to EXP1/EXP2, by (primarily longwave) radiation convergence in clouds in the middle to upper troposphere, particularly near the base of anvil clouds from convection. Heating from radiation convergence continues through anvil clouds to the upper troposphere before changing to be cooling above clouds in the lower stratosphere (e.g., Sherwood et al. 1994). Similar cloud radiative heating profiles have been observed at the DOE ARM sites in the tropical western Pacific (see Fig. 12 of McFarlane et al. 2007). The cloud radiative heating in the middle to upper troposphere as well as latent heating from deep convection (discussed next) result in the warmer temperature in the middle to upper troposphere in the CTRL (Fig. 6a). When the cloud radiative effect is absent

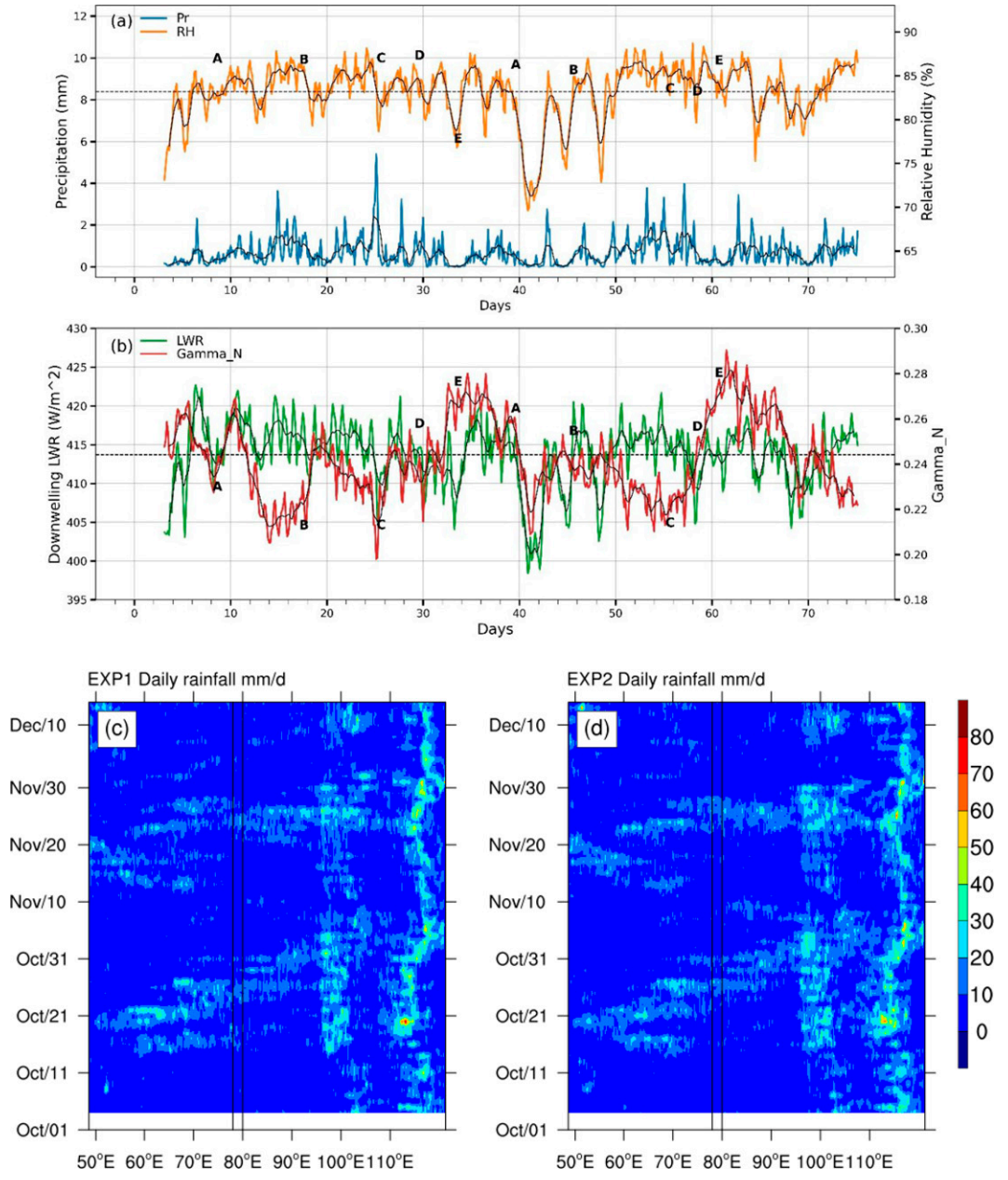

FIG. 5. (a),(b) 3-hourly time series of model physical variables of EXP1 from 1 Oct (day 0) to 15 Dec (day 75) 2011. [The time series starts on day 3 (4 Oct) after the model self-adjustment to forced cloud transparency to radiation.] These results are averaged over blue square box area in Fig. 1. The thin black solid line in the time series of each variable is its eight-value running mean. The uppercase letters A to E are marked at the same date and hour as in the CTRL result in Fig. 3. (c) Time–longitude diagram of EXP1 daily rainfall rate (units: mm day^{-1}) from October to December 2011. (d) As in (c), but for EXP2.

in EXP1/EXP2 the heating in the middle to upper troposphere disappears and its temperature is much cooler.

This heating in the middle to upper troposphere by cloud radiative effect has profound impacts on both the intensity and longevity of deep convection. The warmer temperature from the heating increases the buoyancy of cloudy air in the middle to upper troposphere. This extra buoyancy, in addition to that from cloud latent heat release, accelerates the vertical motion inside convection in the middle to upper troposphere. Accelerated rising near the top of convection creates a vacuum effect in the column that further intensifies and sustains vertical motion and deep convection. The vertical motion profile in this process is shown by the solid line in Fig. 6c. It has a deep layer of strong upward motion in the middle to upper

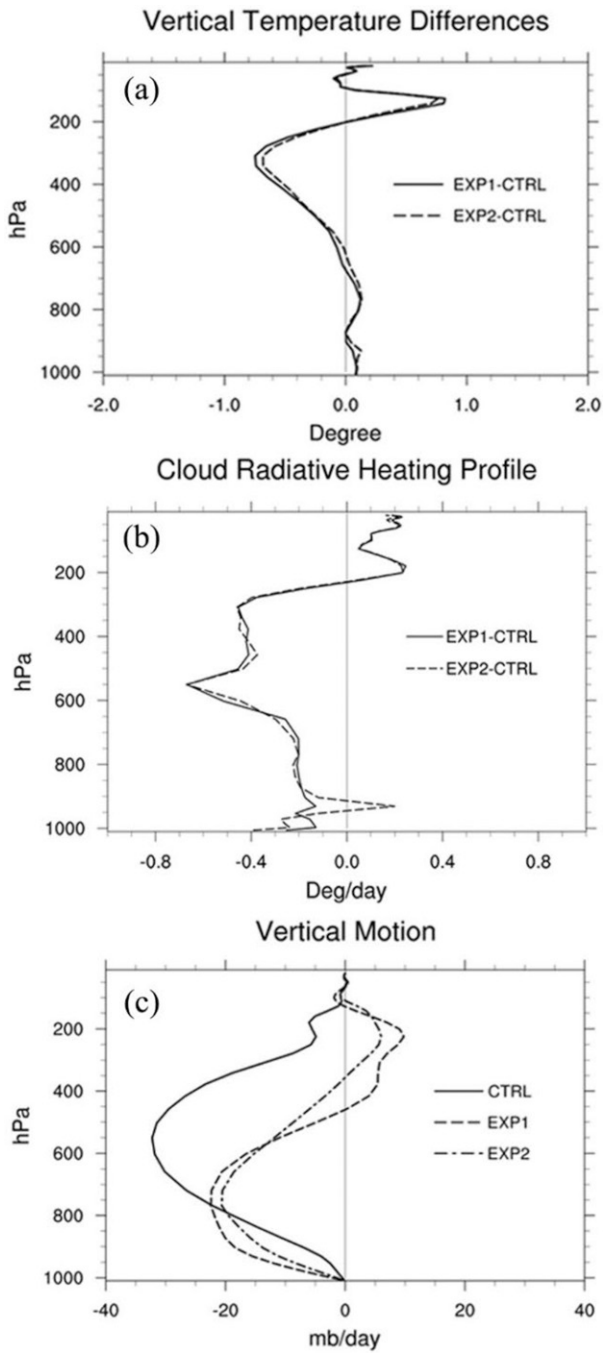

FIG. 6. The difference of (a) vertical temperature profile (units: °C) and (b) cloud radiative heating profile (units: degrees day^{-1}) between the experiments and CTRL. (c) The profile of vertical motion (dp/dt; units: hPa day^{-1}) from the CTRL and experiments.

troposphere with a peak between 500 and 600 hPa. This profile of vertical motion agrees with the observed time-mean profile in DYNAMO (e.g., see Fig. 20 of Johnson and Ciesielski 2013). It is however in utter contrast to that from EXP1 and EXP2, also shown in Fig. 6c, with considerable subsidence in the upper half of the troposphere. Weak upward motion is limited in the lower troposphere, a result indicating mostly shallow clouds (Fig. 5). The absence of deep convection in EXP1/EXP2 indicated by their vertical motion profile (representing primarily the condition in the active phase of the MJO events when deep convection would happen as in the CTRL) is a result of the absence of the cloud radiative effects. In the absence of deep convection, the MJO is missing (Fig. 5).

In Fig. 7, we further compare the variation of vertical motion and RH between the CTRL and EXP1. Figure 7a (CTRL) shows an episode of strong upward motion during the deep convective phase of each of the MJO events. The vertical motion has a "top-heavy" signature, similar to that derived from the ERA-Interim data shown in Fig. 7a of Sobel et al. (2014). This top-heavy profile derived from both the CTRL and ERA-Interim data indicates an acceleration of vertical motion in the middle to upper troposphere. This acceleration could result from the increasing buoyancy and vertical motion (i.e., the vacuum effect) in the upper troposphere by the cloud radiative effects described earlier. It can sustain deep convection by the feedback of increasing and intensifying convection and therefore additional and strong radiative effects in the middle to upper troposphere. Without this cloud radiative (vacuum) effect in EXP1 the upward motion is sporadic, weak, unorganized, and short-lived (Fig. 7b).

c. *Feedback of moisture convergence to cloud radiative effect and deep convection*

Sustaining strong vertical motion and deep convection also requires continuous supplies of abundant moisture. Figures 7c and 7d show the vertical profile of the variation of atmospheric moisture (RH) from the CTRL and EXP1, respectively. In the CTRL, Fig. 7c shows organized episodes of deep layer moisture during the time of strong upward motion and deep convection (w in Fig. 7a). Moist air of RH $>$ 60% extends to 300 hPa. In contrast, RH in EXP1 in Fig. 7d shows much shallower and less humid air at the same time with slightly more moisture confined in the boundary layer of the model (e.g., the average RH from 850 hPa to the surface is 83.23% in EXP1 vs 81.84% in the CTRL). These differences indicate that the deep layer of high moisture content in the CTRL is also a result of the cloud radiative effect because it is the only difference in the model settings between the CTRL and EXP1. Additional evidence supporting this notion is from the horizontal convergence of moisture shown in Fig. 7e. The vertically integrated moisture convergence in the CTRL (negative value in Fig. 7e) is in phase with the variation of RH in Fig. 7c and the vertical motion in Fig. 7a. Intense vertically integrated moisture convergence occurred during deep convection when the cloud radiative effect and its generated vacuum forcing are the strongest. In contrast, there is little evidence of intraseasonal variation of moisture convergence in EXP1 (Fig. 7f). Because both the CTRL and EXP1 are using the same lateral and lower boundary conditions and the cloud radiative effect only appears when deep convection has occurred in the CTRL, these differences in vertically integrated horizontal convergence of moisture between the CTRL and EXP1 are likely not a result of the large-scale circulation

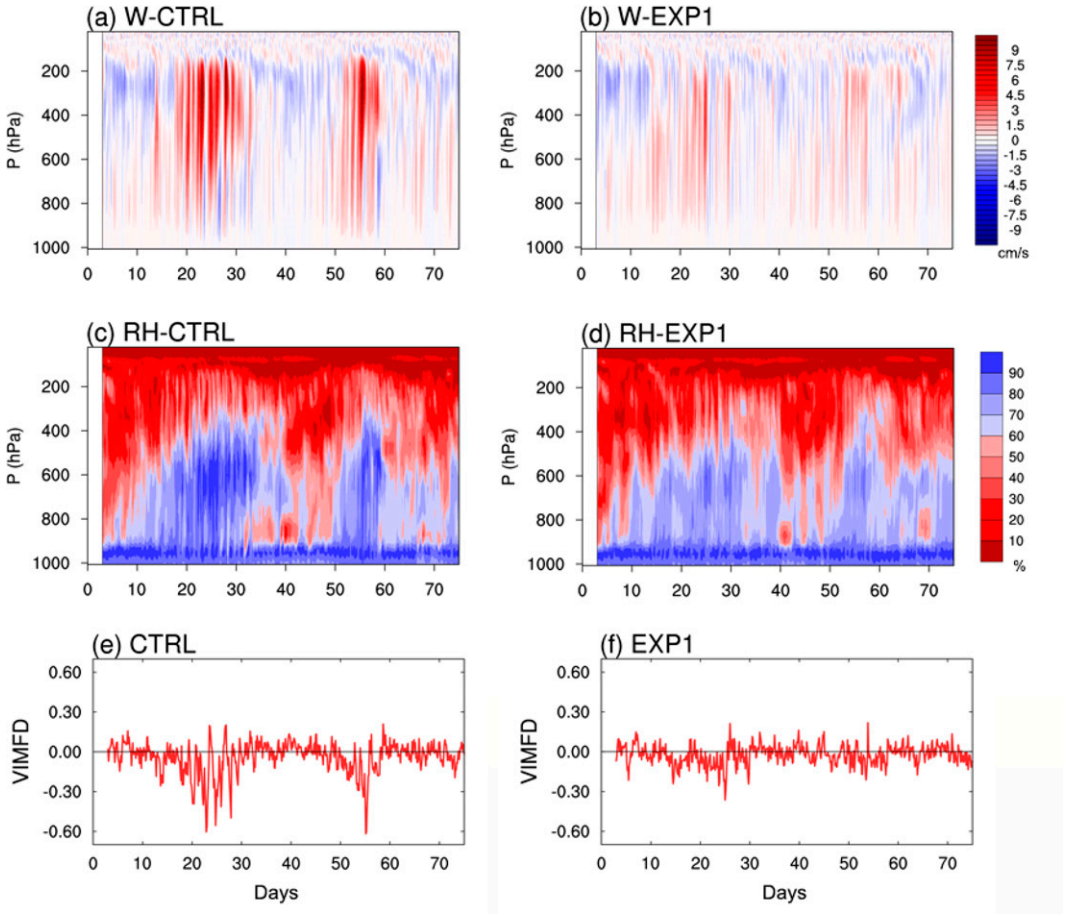

FIG. 7. (a),(c),(e) The CTRL results of 3-hourly vertical motion (cm s^{-1}), RH (%; with respect to ice), and vertically integrated (surface to 500 hPa) horizontal moisture flux divergence (VIMFD; g m^{-2} s^{-1}), respectively. (b),(d),(f) As in (a), (c), and (e), but from EXP1.

anomalies (or strong moisture convergence would have been present in EXP1, too). They should be a result consistent with (i.e., required by) the cloud radiative effect in the CTRL.

An explanation of the connection of the cloud radiative effect and the large-scale moisture convergence is that when the rising motion strengthens in the middle to upper troposphere by the cloud radiative effect, primarily the heating from net vertical convergence of longwave radiation and the subsequent vacuum effect, there will be a demand for the air mass in the lower troposphere to rise and fill the "vacuum" created by the accelerated rising motion in the middle to upper troposphere (Fig. 6c). This enhanced rising motion in the middle to upper troposphere is shown by the top-heavy rising motion profile in Fig. 7a, and also in Fig. 7a of Sobel et al. (2014) derived from reanalysis data. The induced rising motion in the middle to lower troposphere by the vacuum effect requires large-scale mass convergence to sustain the horizontal pressure/mass balance. This mass/moisture convergence (Fig. 7e) describes a positive feedback from the large-scale circulation to the cloud radiative effect that helps sustain deep convection and the MJO. When the cloud radiative effect is excluded in EXP1 this feedback is missing and deep convection cannot be sustained (Figs. 6c and 7b). Subsequently, the troposphere is drier, especially the upper troposphere (Fig. 7d), and no MJO appears (Fig. 5).

The surface evaporation effect on atmospheric moisture and convection during the MJO events is examined from our surface energy budget analysis. The results are shown in Fig. 8a. During the period of strong horizontal convergence of moisture concurring with the deep convection of the MJO in the CTRL (Figs. 7a,e), the strengthening winds in the lower troposphere also increase the surface evaporation. Because the net radiation at the surface is reduced, due largely to the decrease of solar radiation reaching the surface (Fig. 8a), the increase of surface evaporation could be largely driven by winds and also the drying of the near-surface layer by strong upward vertical moisture flux (see Fig. 13 of WSZSYZ). Evaporative cooling of hydrometeors during deep convection and intense Pr also encourages surface sensible heat flux (Fig. 8a). When the cloud radiative effect is suppressed in EXP1, its energy budget at the surface (Fig. 8b) shows only minor fluctuations during the time of the MJO events.

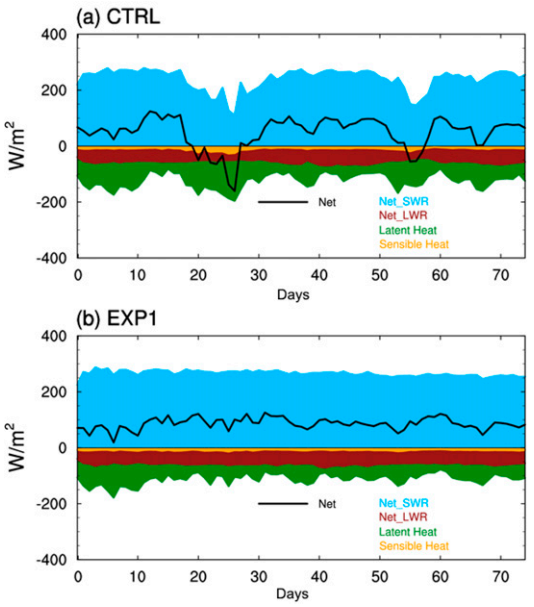

FIG. 8. Surface energy budget of (a) CTRL and (b) EXP1.

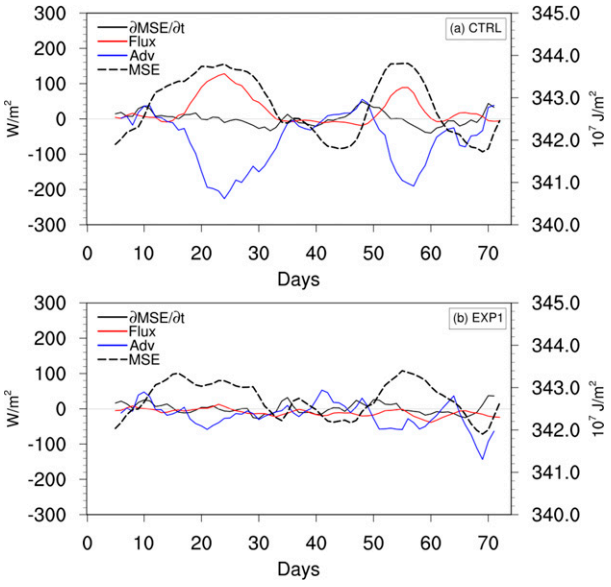

FIG. 9. Area-averaged (over study area in the blue square in Fig. 1) time series (after a 5-day moving average) of mass-weighted column-integrated MSE budget terms derived from (a) CTRL and (b) EXP1. "Flux" (red solid line, units: W m^{-2}) is the source sum of net radiation and surface sensible and latent heat fluxes, and "Adv" (blue solid line, units: W m^{-2}) is the sum of horizontal and vertical advection of MSE. Negative Adv indicates converging flux into the study region. The tendency of MSE, ∂MSE/∂t, is shown by the black solid line (units: W m^{-2}), and the temporal variation of column-integrated MSE is show by the black dashed line (units: 10^7 J m^{-2}).

d. *A self-destruction mission of deep convection—The closure*

Deep convection changes the atmospheric temperature lapse rate through both the cloud radiative effects and subsequent warming in convection-induced large-scale descent (heating from adiabatic compression in the overturning circulation). In doing so, it is stabilizing the atmosphere, making its lapse rate stable with respect to the content of moisture (Manabe and Strickler 1964). After a period of deep convection, the atmosphere will become stabilized with respect to the moisture so that no additional deep convection is required (Fig. 4). At that point, convection weakens and, subsequently, the moistening process weakens from the weakening of both horizontal and vertical convergence of moisture (e.g., Fig. 7e; see also Fig. 13 of WSZSYZ). This marks the end of the active convective phase of the two MJO events (Figs. 3 and 7a,c).

During the decay stage of the MJO events, the atmospheric moisture is continuously depleted by weak/shallow convection (Figs. 3a,b and 7c) while the lapse rate is becoming steeper by radiation processes at the surface and in the atmosphere (also consistent with the decrease of moisture). The increasing solar heating and upward LWR at the surface (Fig. 8a) play a major role in warming the lower troposphere while the net LWR in the upper troposphere without clouds will decrease its temperature (Figs. 6a,b).

These processes are also depicted in Fig. 4 by the change of the tropospheric condition in the Γ_N–RH diagram. At the peak of convection, the troposphere of both observed and the CTRL is at the state marked by C when the atmosphere is high in moisture (large RH) and at the least steep lapse rate (small Γ_N; i.e., highest stability). In this stable condition, no additional deep convection is required. The condition shifts from C to D, showing the collapse of deep convection and related horizontal moisture convergence (Fig. 7e). The end of this cycle also presents the potential for the development of another event when new embryos of intraseasonal oscillation form in the radiative–convective system over the tropical warm water regions.

e. *Cloud radiative effect on moist static energy*

Atmospheric moist static energy (MSE $= h = c_pT + gz + L_vq_v - L_fq_i$, where c_p is the specific heat at constant pressure, g is gravity, L_v is the latent heat of vaporization, L_f is the latent heat of freezing, and q_v and q_i are atmospheric vapor and ice mixing ratio, respectively) has often been used in diagnostics of variations of energy state during the development of the MJO (e.g., Lin and Mapes 2004; Andersen and Kuang 2012; Kim et al. 2014; Sobel et al. 2014; Wang et al. 2015). The MSE variation and the variations of energy flux term and advective term in MSE budget for the CTRL and EXP1 are shown in Figs. 9a and 9b, respectively. The flux term ("Flux" shown by the red line in Fig. 9) measures local sources of MSE and is the sum of column-integrated radiation flux and surface sensible and latent heat fluxes. The advective term ("Adv" blue line in Fig. 9) measures the effect of large-scale circulation on local MSE and is the sum of column-integrated horizontal and vertical advection of MSE. These terms were calculated using the methods detailed in Sobel et al. (2014).

Figure 9 shows large differences in the budget of MSE between the CTRL and EXP1 (cf. Figs. 9a,b) in the active phase of deep convection in the two MJO events. In the CTRL, the flux term increased sharply when deep convection occurred (see Fig. 3a for the timing). This increase is a result of the increase of RH and the increase of cloud radiative heating (Figs. 3a,b and 6b) when it is amplifying convection. Meanwhile, the Adv term in the MSE budget shows strong inward advection of or converging (negative value) MSE, a result indicating the support of large-scale circulation to intensifying deep convection fueled by the vacuum effect of the cloud radiative heating (Fig. 6). This sharp increase of advective effect on the MSE of the study region is consistent with the large-scale moisture convergence shown in Fig. 7e during the convective phase of the MJO events. It is particularly important to notice that the peak value of the converging Adv term in the study region has a slight time lag relative to the peak value of the flux/source term, especially distinct in the second MJO event from 20 November (day 50) to 1 December (day 60). Although it is inconclusive because only two cases are examined here, this phase lag suggests that the processes of large-scale circulation that supported the energy needs of the MJO development are responses to, and hence slightly behind, the processes described in the source term, primarily the column-integrated radiation flux from the cloud radiative forcing. When this forcing weakened after the stabilization of the atmosphere by deep convection (section 4d) the advective effect of large-scale circulation also weakened and faded.

This notion that the cloud radiative effect is driving the development of these MJO events is further supported by the result shown in Fig. 9b; that is, when the cloud radiative effect is absent in EXP1 only weak intraseasonal variations exist (also see Fig. 5). These results of MSE budget and the variations of the individual elements constituting the MSE (Figs. 3 and 5) suggest that in these MJO cases processes in large-scale circulation such as advection play an important role to supply moisture and energy and elevate/prolong the MJO development. The condition (an instability) that activates the large-scale circulation to play this role is primarily developed by the cloud radiative forcing (the vacuum effect; sections 4b and 4c).

The weak MSE variation of intraseasonal time scale in Fig. 9b is consistent with the low-level cloudiness in Figs. 5c and 5d, and also the result of Hu and Randall (1994). As we have discussed earlier, this weak yet visible variation in low-level cloudiness and associated MSE describes a presence, or an embryo, of the intraseasonal oscillation that can exist in the tropical atmosphere from interactions of radiation and convection over warm waters. The results of this study show that the cloud radiative effect is a required forcing that can grow/amplify some of the intraseasonal anomalies of convection under some specific conditions. In this process, the cloud radiative effect and its feedbacks including those from advections of MSE by large-scale circulations can elevate and further concentrate the atmospheric energy to a much high value/state in regions where MJO can take place.

5. Summary and concluding remarks

Two observed MJO events during the DYNAMO IOP are examined for a plausible causal mechanism of the MJO development. The mechanism is the cloud radiative effect. This effect was not included in the original work of Hu and Randall (1994), who showed in their one-dimensional models that intraseasonal oscillations can arise as a result of destabilization of the atmosphere by radiation and stabilization by convection over warm waters in the tropics. The oscillations are rather weak, however, and their related convection is confined to the lower troposphere. Their connection to the observed MJO events was not clear. In the follow-up work of Hu and Randall (1995), the cloud radiative effect was included through a parameterization in the one-dimensional context. While stronger intraseasonal oscillations occurred in the results the parameterization limited the potential of using the results to gain understanding of the cloud radiative effect in the development of the oscillations. This present work using a regional model and observed MJO events shows that the intraseasonal oscillations in radiative–convective systems without considering cloud radiative effect could be the embryos of MJO. They can grow and develop into full strength MJO by cloud radiative effects and feedbacks.

Those effects and feedbacks are identified by the differences between the model control simulation of the MJO events and simulations from the same model after the cloud radiative effects are eliminated by making the clouds transparent to both the solar and longwave radiation.

The absence of the MJO events in the model experiments with no cloud-radiation effects confirms the essential role of those effects in the MJO development. The key role of the cloud radiative effects is the heating from the shortwave absorption within anvil clouds in the upper troposphere and the net convergence of LWR in the middle to upper troposphere through the anvil clouds resulted from detrainment of deep convection. That heating drives two processes. First, it adds extra buoyancy and accelerates the rising motion of cloud/convection air in the middle to upper troposphere. This vertical acceleration in the middle to upper troposphere creates a vacuum effect that requires more and stronger deep convection to develop. Second, the requirement by mass balance demands and drives a strong increase of large-scale horizontal and vertical convergence of mass. Horizontal mass, moisture, and energy convergence strengthens deep convection and, with the feedback from continuing convection and its elevated cloud radiative effect, creates conditions that can perpetuate deep convection (to grow the embryo of intraseasonal oscillation) and MJO development.

These processes arising from the cloud radiative heating in the middle to upper troposphere weaken after a period during which the heating has raised the upper troposphere temperature and stabilized the temperature profile such that it supports no further deep convection. As shown in our results, convection weakens and precipitation decreases commencing at the time when the atmospheric lapse rate reaches its minimum value. Collapsing deep convection reduces the amount of anvil clouds and the cloud radiative effect. The subsequent reduction and absence of the vacuum effect in the upper

troposphere diminishes deep convection and the MJO cycle is completed.

Contemporaneously, a reversed radiative heating profile in the atmosphere with weak/shallow convection (i.e., increased solar heating at the surface and lower troposphere and net LWR cooling in the upper troposphere) resumes and starts destabilizing the troposphere again. With the increase of moisture from surface evaporation this destabilization intensifies. Embryos of intraseasonal oscillation form in these radiative–convective processes, waiting for proper conditions to grow and develop.

As the observations have indicated, "proper conditions" for development of deep convection do not occur often and MJO events are rather irregular (e.g., Hu et al. 2009), in contrast to the regular intraseasonal oscillation in pure radiative–convection systems (Hu and Randall 1994, 1995). This difference could be attributed to many other processes concurring and interfering with the cloud radiative effect (e.g., Zhang et al. 2020). A key element in this interference is the motion field and waves occurring with or prior to the MJO development. For example, waves prior to or excited by deep convection can distort connections between the upper and lower troposphere during deep convection and alter the vacuum effect. They could also interrupt the engagement of the large-scale circulation (moisture and energy) support in MJO development. Determining in what conditions such processes may disrupt, and in what conditions they would enhance, MJO development started or driven by the cloud radiative effect remains to be examined in order to further advance our understanding of the MJO.

A related issue, not addressed in this study, is what role the cloud radiative effect may have played in the propagation of the MJO. MJO propagation is a rather perplexing subject. As shown in Fig. 2, the MJO complex during the DYNAMO contained a wide range of spectrum of waves that propagated both eastward and westward although the MJO signal proceeded eastward. As shown by the energy spectrum of waves in the wavelength–frequency diagram in Fig. S1 in the online supplemental material, there are gravity waves emanating from deep convection in the MJO. Those propagating westward have more energy, as also clearly shown in Fig. 2. Figure S1 also shows eastward propagating MJO signal in the CTRL result as in the observed. When the cloud radiative effect is suppressed in EXP1 its result shows no MJO signal and more energy in high-frequency (diurnal to 2 days per cycle) gravity waves. It is interesting to note that quasi-stationary intraseasonal oscillations remain in the model experiments without the cloud radiative effects. These results show wave components and their changes with and without the cloud radiative effect. The roles of the cloud radiative effect and its interaction with large-scale circulation in the development of those waves and their propagation will be studied separately.

Acknowledgments. We thank four anonymous reviewers whose comments have helped improve this work in both its contents and clarity. Qi Hu thanks Dr. George Kiladis of the University of Colorado for helpful discussions in the early phase of this work. Thanks also go to Dr. Hua Guo for help in making several figures. The computations in this study were performed on facilities of the Holland Computing Center of the University of Nebraska–Lincoln. This work was partially supported by NSF grants AGS-1924679 to the University of Nebraska–Lincoln and AGS-1543932 to Columbia University, and by the USDA Cooperative Research Project NEB-38-088.

Data availability statement. Datasets in group 1 of this research are available in the public domain (https://www.ecmwf.int/en/forecasts/dataset/ecmwf-reanalysis-v5). Datasets in Group 2 of this research are described in detail in Johnson and Ciesielski (2013) and Ciesielski et al. (2014) and are available at the websites given in their publications. Data generated during this research are available from the authors upon request.

REFERENCES

Andersen, J. A., and Z. Kuang, 2012: Moist static energy budget of MJO-like disturbances in the atmosphere of a zonally symmetric aqua-planet. *J. Climate*, **25**, 2782–2804, https://doi.org/10.1175/JCLI-D-11-00168.1.

Arakawa, A., and J. M. Chen, 1987: Closure assumptions in the cumulus parameterization problem. *Short- and Medium-Range Numerical Prediction: Collection of Papers Presented at the WMO/IUGG NWP Symposium*, T. Matsuno, Eds., JMA, 107–131.

Benedict, J. J., B. Medeiros, A. C. Clement, and J. G. Olson, 2020: Investigating the role of cloud-radiation interactions in subseasonal tropical disturbances. *Geophys. Res. Lett.*, **47**, e2019GL086817, https://doi.org/10.1029/2019GL086817.

Bladé, I., and D. L. Hartmann, 1993: Tropical intraseasonal oscillations in a simple nonlinear model. *J. Atmos. Sci.*, **50**, 2922–2939, https://doi.org/10.1175/1520-0469(1993)050<2922:TIOIAS>2.0.CO;2.

Bony, S., and K. A. Emanuel, 2005: On the role of moist processes in tropical intraseasonal variability: Cloud–radiation and moisture–convection feedbacks. *J. Atmos. Sci.*, **62**, 2770–2789, https://doi.org/10.1175/JAS3506.1.

Cahill, K., 2013: Differential equations. *Physical Mathematics.* Cambridge University Press, 223–295.

Ciesielski, P. E., and Coauthors, 2014: Quality-controlled upper-air sounding dataset for DYNAMO/CINDY/AMIE: Development and corrections. *J. Atmos. Oceanic Technol.*, **31**, 741–764, https://doi.org/10.1175/JTECH-D-13-00165.1.

Duan, Y., H. Liu, W. Yu, L. Liu, G. Yang, and B. Liu, 2019: The onset of the Indonesian–Australian summer monsoon triggered by the first-branch eastward-propagating Madden–Julian Oscillation. *J. Climate*, **32**, 5453–5470, https://doi.org/10.1175/JCLI-D-18-0513.1.

Emanuel, K. A., 1987: An air–sea interaction model of intraseasonal oscillations in the tropics. *J. Atmos. Sci.*, **44**, 2324–2340, https://doi.org/10.1175/1520-0469(1987)044<2324:AASIMO>2.0.CO;2.

Hersbach, H., and Coauthors, 2020: The ERA5 global reanalysis. *Quart. J. Roy. Meteor. Soc.*, **146**, 1999–2049, https://doi.org/10.1002/qj.3803.

Hu, Q., 1992: Low-frequency oscillations in radiative-convective models. Ph.D. dissertation, Dept. of Atmospheric Science, Colorado State University, 196 pp.

——, and D. A. Randall, 1994: Low-frequency oscillations in radiative-convective systems. *J. Atmos. Sci.*, **51**, 1089–1099, https://doi.org/10.1175/1520-0469(1994)051<1089:LFOIRC>2.0.CO;2.

——, and ——, 1995: Low-frequency oscillations in radiative-convective systems. Part II: An idealized model. *J. Atmos. Sci.*, **52**, 478–490, https://doi.org/10.1175/1520-0469(1995)052<0478:LFOIRC>2.0.CO;2.

——, Z. N. Liang, and M. W. Hoffman, 2009: Detecting source regions of wave activities in the tropical atmosphere by applying beamforming to interpolated data grids. *J. Atmos. Oceanic Technol.*, **26**, 270–280, https://doi.org/10.1175/2008JTECHA1121.1.

Huffman, G. J., and Coauthors, 2007: The TRMM Multisatellite Precipitation Analysis (TMPA): Quasi-global, multiyear, combined-sensor precipitation estimates at fine scales. *J. Hydrometeor.*, **8**, 38–55, https://doi.org/10.1175/JHM560.1.

Johnson, R. H., and P. E. Ciesielski, 2013: Structure and properties of Madden–Julian oscillations deduced from DYNAMO sounding arrays. *J. Atmos. Sci.*, **70**, 3157–3179, https://doi.org/10.1175/JAS-D-13-065.1.

Khairoutdinov, M. F., and D. A. Randall, 2006: High resolution simulation of shallow-to-deep convection over land. *J. Atmos. Sci.*, **63**, 3421–3436, https://doi.org/10.1175/JAS3810.1.

——, and K. A. Emanuel, 2018: Intraseasonal variability in a cloud-permitting near-global equatorial aquaplanet model. *J. Atmos. Sci.*, **75**, 4337–4355, https://doi.org/10.1175/JAS-D-18-0152.1.

Kim, D., and Coauthors, 2009: Application of MJO simulation diagnostics to climate models. *J. Climate*, **22**, 6413–6436, https://doi.org/10.1175/2009JCLI3063.1.

——, A. H. Sobel, and I.-S. Kang, 2011: A mechanism denial study on the Madden–Julian Oscillation. *J. Adv. Model. Earth Syst.*, **3**, M12007, https://doi.org/10.1029/2011MS000081.

——, and Coauthors, 2014: Process-oriented MJO simulation diagnostic: Moisture sensitivity of simulated convection. *J. Climate*, **27**, 5379–5395, https://doi.org/10.1175/JCLI-D-13-00497.1.

Lau, K. M., and L. Peng, 1987: Origin of the low-frequency (intraseasonal) oscillations in the tropical atmosphere: Part I: Basic theory. *J. Atmos. Sci.*, **44**, 950–972, https://doi.org/10.1175/1520-0469(1987)044<0950:OOLFOI>2.0.CO;2.

Lin, J.-L., and B. E. Mapes, 2004: Radiation budget of the tropical intraseasonal oscillation. *J. Atmos. Sci.*, **61**, 2050–2062, https://doi.org/10.1175/1520-0469(2004)061<2050:RBOTTI>2.0.CO;2.

Ma, D., and Z. Kuang, 2011: Modulation of radiative heating by the Madden–Julian Oscillation and convectively coupled Kelvin waves as observed by CloudSat. *Geophys. Res. Lett.*, **38**, L21813, https://doi.org/10.1029/2011GL049734.

——, and ——, 2016: A mechanism-denial study on the Madden–Julian Oscillation with reduced interference from mean state changes. *Geophys. Res. Lett.*, **43**, 2989–2997, https://doi.org/10.1002/2016GL067702.

Madden, R. A., and P. R. Julian, 1971: Detection of a 40–50 day oscillation in the zonal wind in the tropical Pacific. *J. Atmos. Sci.*, **28**, 702–708, https://doi.org/10.1175/1520-0469(1971)028<0702:DOADOI>2.0.CO;2.

Maloney, E. D., and D. L. Hartmann, 2000: Modulation of hurricane activity in the Gulf of Mexico by the Madden–Julian Oscillation. *Science*, **287**, 2002–2004, https://doi.org/10.1126/science.287.5460.2002.

——, A. H. Sobel, and W. M. Hannah, 2010: Intraseasonal variability in an aquaplanet general circulation model. *J. Adv. Model. Earth Syst.*, **2** (2), https://doi.org/10.3894/JAMES.2010.2.5.

Manabe, S., and R. F. Strickler, 1964: Thermal equilibrium of the atmosphere with a convective adjustment. *J. Atmos. Sci.*, **21**, 361–385, https://doi.org/10.1175/1520-0469(1964)021<0361:TEOTAW>2.0.CO;2.

McFarlane, S. A., J. H. Mather, and T. P. Ackerman, 2007: Analysis of tropical radiative heating profiles: A comparison of models and observations. *J. Geophys. Res.*, **112**, D14218, https://doi.org/10.1029/2006JD008290.

Miura, H., M. Satoh, T. Nasuno, A. T. Noda, and K. Oouchi, 2007: A Madden–Julian Oscillation event realistically simulated by a global cloud-resolving model. *Science*, **318**, 1763–1765, https://doi.org/10.1126/science.1148443.

Neelin, J. D., I. M. Held, and K. H. Cook, 1987: Evaporation–wind feedback and low frequency variability in the tropical atmosphere. *J. Atmos. Sci.*, **44**, 2341–2348, https://doi.org/10.1175/1520-0469(1987)044<2341:EWFALF>2.0.CO;2.

Ray, P., and C. Zhang, 2010: A case study of the mechanics of extratropical influence on the initiation of the Madden–Julian oscillation. *J. Atmos. Sci.*, **67**, 515–528, https://doi.org/10.1175/2009JAS3059.1.

Raymond, D. J., 2001: A new model of the Madden–Julian oscillation. *J. Atmos. Sci.*, **58**, 2807–2819, https://doi.org/10.1175/1520-0469(2001)058<2807:ANMOTM>2.0.CO;2.

Sherwood, S. C., V. Ramanathan, T. P. Barnett, M. K. Tyree, and E. Roeckner, 1994: Response of an atmospheric general circulation model to radiative forcing of tropical clouds. *J. Geophys. Res.*, **99**, 20 829–20 845, https://doi.org/10.1029/94JD01632.

Skamarock, W. C., and Coauthors, 2008: A description of the Advanced Research WRF version 3. NCAR Tech. Note NCAR/TN-475+STR, 125 pp., http://dx.doi.org/10.5065/D68S4MVH.

Sobel, A. H., and E. D. Maloney, 2012: An idealized semi-empirical framework for modeling the Madden–Julian oscillation. *J. Atmos. Sci.*, **69**, 1691–1705, https://doi.org/10.1175/JAS-D-11-0118.1.

——, ——, G. Bellon, and D. M. Frierson, 2010: Surface fluxes and tropical intraseasonal variability: A reassessment. *J. Adv. Model. Earth Syst.*, **2** (1), https://doi.org/10.3894/JAMES.2010.2.2.

——, S. Wang, and D. Kim, 2014: Moist static energy budget of the MJO during DYNAMO. *J. Atmos. Sci.*, **71**, 4276–4291, https://doi.org/10.1175/JAS-D-14-0052.1.

Stephens, G. L., and P. J. Webster, 1979: Sensitivity of radiative forcing to variable cloud and moisture. *J. Atmos. Sci.*, **36**, 1542–1556, https://doi.org/10.1175/1520-0469(1979)036<1542:SORFTV>2.0.CO;2.

Takayabu, Y. N., T. Iguchi, M. Kachi, A. Shibata, and H. Kanzawa, 1999: Abrupt termination of the 1997–98 El Niño in response to a Madden–Julian oscillation. *Nature*, **402**, 279–282, https://doi.org/10.1038/46254.

Waliser, D. E., K. M. Lau, W. Stern, and C. Jones, 2003: Potential predictability of the Madden–Julian oscillation. *Bull. Amer. Meteor. Soc.*, **84**, 33–50, https://doi.org/10.1175/BAMS-84-1-33.

Wang, B., 1988: Dynamics of tropical low-frequency waves: An analysis of the moist kelvin wave. *J. Atmos. Sci.*, **45**, 2051–2065, https://doi.org/10.1175/1520-0469(1988)045<2051:DOTLFW>2.0.CO;2.

——, 2005: Theory. *Intraseasonal Variability in the Atmosphere–Ocean Climate System*, 2nd ed., W. K. M. Lau and D. E. Waliser, Eds., Springer, 307–360.

——, and T. Li, 1994: Convective interaction with boundary-layer dynamics in the development of tropical intraseasonal system. *J. Atmos. Sci.*, **51**, 1386–1400, https://doi.org/10.1175/1520-0469(1994)051<1386:CIWBLD>2.0.CO;2.

Wang, S., A. H. Sobel, and Z. Kuang, 2013: Cloud-resolving simulation of TOGA-COARE using parameterized large-scale dynamics. *J. Geophys. Res. Atmos.*, **118**, 6290–6301, https://doi.org/10.1002/jgrd.50510.

——, ——, F. Zhang, Y. Q. Sun, Y. Yue, and L. Zhou, 2015: Regional simulation of the October and November MJO events observed during the CINDY/DYNAMO field campaign at gray zone resolution. *J. Climate*, **28**, 2097–2119, https://doi.org/10.1175/JCLI-D-14-00294.1.

——, ——, and J. Nie, 2016: Modeling the MJO in a cloud-resolving model with parameterized large-scale dynamics: Vertical structure, radiation, and horizontal advection of dry air. *J. Adv. Model. Earth Syst.*, **8**, 121–139, https://doi.org/10.1002/2015MS000529.

Webster, P. J., 1983: Mechanisms of monsoon low-frequency variability: Surface hydrological effects. *J. Atmos. Sci.*, **40**, 2110–2124, https://doi.org/10.1175/1520-0469(1983)040<2110:MOMLFV>2.0.CO;2.

Wheeler, M. C., and J. L. McBride, 2005: Australian–Indonesian monsoon. *Intraseasonal Variability in the Atmosphere–Ocean Climate System*, 2nd ed., W. K.-M. Lau and D. E. Waliser, Eds., Springer, 125–174.

Yoneyama, K., C. Zhang, and C. N. Long, 2013: Tracking pulses of the Madden–Julian oscillation. *Bull. Amer. Meteor. Soc.*, **94**, 1871–1891, https://doi.org/10.1175/BAMS-D-12-00157.1.

Zhang, B., R. J. Kramer, and B. J. Soden, 2019: Radiative feedbacks associated with the Madden–Julian oscillation. *J. Climate*, **32**, 7055–7065, https://doi.org/10.1175/JCLI-D-19-0144.1.

Zhang, C., Á. F. Adames, B. Khouider, B. Wang, and D. Yang, 2020: Four theories of the Madden–Julian Oscillation. *Rev. Geophys.*, **58**, e2019RG000685, https://doi.org/10.1029/2019RG000685.